Kodaikanal Obs. Bull. Ser. A (1980) 3, 6-16

FLOW OF GAS ALONG A MAGNETIC FIELD WITH TIME-DEPENDENT GEOMETRY

S. S. HASAN and P. VENKATAKRISHNAN

ABSTRACT

The flow of gas along a magnetic field with time dependent geometry has been studied. It is seen that the velocity of the flow in the direction of the magnetic field depends both on the magnitude of the velocity of flow perpendicular to the field as well as on its spatial variation. Further, the nature of the flow is not very sensitive to the choice of base temperature and polytropic index. The application of this study to magnetofluid dynamic flow on the Sun is discussed.

Key words: fluid dynamics—one dimensional unsteady flow; astrophysics—Sun—magnetofluid dynamics

1. Introduction

The study of gas flow along a magnetic field with time-dependent geometry is of considerable interest to astrophysics. A wide variety of flows have been observed on the Sun, which appear to be channelled by magnetic fields. The present study was undertaken mainly to understand the behaviour of such flows when the configuration of the magnetic field changes with time.

Among the various complexities which exist for flows in the solar atmosphere are the presence of gravity, the curvature of magnetic fields, the compressibility of gas, partial ionization of matter and energy losses and gains in the guise of radiation, conduction and heating by waves. To study flows including all these features is a formidable task. There is also the danger of swamping essential information in a deluge of details. As a first step, therefore, we have concentrated on the effect of the change in geometry of the field on the motion of gas along it For this, we prescribe the velocity of a field line normal to itself and integrate the equation of motion parallel to the field. The necessary coupling between the normal and parallel velocities is provided by the continuity equation where the full effects of compressibility have been incorporated. The energy equation is replaced by a polytropic law to simplify the mathematical analysis.

2. Initial Geometry of the Magnetic Field

It is assumed that the magnetic field is in the y-z plane, with gravity acting in the negative z-direction. It is convenient to transform to a curvilinear system of coordinates consisting of unit vectors **s** and **n** in the direction of the tangent and the outward normal to the field line respectively. The main equations are considered in this curvilinear system whereas, for determining the stream geometry as a function of time, it is more convenient to consider cartesian coordinates. The space and time derivatives of the unit vectors **s** and **n** are given by:

$$\frac{\partial \mathbf{s}}{\partial t} = -\frac{\partial \theta}{\partial t}\mathbf{n}\,;\quad \frac{\partial \mathbf{s}}{\partial s} = \frac{\mathbf{n}}{R}\,;\quad \frac{\partial \mathbf{s}}{\partial n} = \frac{\mathbf{n}}{R_n}$$

$$\frac{\partial \mathbf{n}}{\partial t} = -\frac{\partial \theta}{\partial t}\mathbf{s}\,;\quad \frac{\partial \mathbf{n}}{\partial s} = -\frac{\mathbf{n}}{R}\,;\quad \frac{\partial \mathbf{n}}{\partial n} = -\frac{\mathbf{s}}{R_n}\,; \qquad (2.1)$$

where θ is the angle between the field line and the vertical and R and R_n are the radii of curvature of the line and its orthogonal respectively.

The initial magnetic configuration is assumed to have a potential form given by:

$$B_y = B_0 e^{-kx} \sin ky\,; \quad B_x = B_0 e^{-kx} \cos ky\,; \tag{2.2}$$

where B_y and B_x are the horizontal and vertical components of the field and k is a constant which represents the degree of curvature of the line. The equation of a field line is easily determined as:

$$\sin (ky) = \sin (ky_0)\, e^{kx}\,, \tag{2.3}$$

where y_0 is the value of y at the base of the field line. We also see that

$$\begin{aligned} \theta &= ky\,; \\ R &= (k \sin ky)^{-1}\,; \\ R_n &= (k \cos ky)^{-1}\,. \end{aligned} \tag{2.4}$$

3. The Magnetofluid Dynamical Equations

The magnetofluid dynamical equations for an infinitely conducting fluid are

$$\frac{\partial \rho}{\partial t} + \nabla .\, (\rho V) = 0 \tag{3.1a}$$

and

$$\rho \left(\frac{\partial V}{\partial t} + V .\, \nabla\, V \right) = - \nabla p + \rho g + f\,, \tag{3.1b}$$

where ρ is the density, V the velocity, p the pressure, g the acceleration due to gravity and f represents all other body forces, for example, the Lorentz force due to the magnetic field. The energy equation is replaced by the polytropic law,

$$a^2 = \Gamma RT, \tag{3.1c}$$

where a is the sound speed, R is the gas constant, T is the temperature and Γ is the polytropic index which is unity for the isothermal case.

As mentioned earlier, we shall consider only the equation of motion parallel to the field and prescribe V_n, the velocity normal to the field, in place of the lateral equation of motion. (For a similar procedure in the context of coronal magnetic reconnection, see Kopp and Pneuman, 1976). The equation of motion along the field line can now be written as:

$$\frac{\partial V_s}{\partial t} + V_s \frac{\partial V_s}{\partial s} + V_n \frac{\partial V_s}{\partial n} = - \frac{1}{\rho} \frac{\partial p}{\partial s} - g \cos \theta + V_n \frac{\partial \theta}{\partial t} + \frac{V_s V_n}{R} + V_n^2 \frac{\partial \theta}{\partial n}\,, \tag{3.2}$$

where V_s is the velocity parallel to the field and p is the pressure. We can recast equation (3.2) in a frame of reference moving with the field line as:

$$\frac{DV_s}{Dt} + V_s \frac{DV_s}{Ds} = - \frac{1}{\rho} \frac{Dp}{Ds} - g \cos \theta + V_n \frac{D\theta}{Dt} + \frac{V_n V_s}{R}\,, \tag{3.3}$$

using the following operator relationships:

$$\frac{D}{Ds} = \frac{\partial}{\partial s} \tag{3.3a}$$

and

$$\frac{D}{Dt} = \frac{\partial}{\partial t} + V_n \frac{\partial}{\partial n}\,. \tag{3.3b}$$

The equation of continuity (3.1a) can likewise be written as:

$$\frac{DV_s}{Ds} + \frac{D \ln \rho}{Dt} + V_s \frac{D \ln \rho}{Ds} + V_s \frac{\partial \theta}{\partial n} - \frac{V_n}{R} + \frac{\partial V_n}{\partial n} = 0\,. \tag{3.4}$$

Equations (3.3) and (3.4), along with equation (3.1c), form a hyperbolic set of partial differential equations and therefore possess two real characteristics. The equations of the characteristics in the t – s plane are

$$\left(\frac{dt}{ds}\right)_+ = \frac{1}{u+a} \text{ and } \left(\frac{dt}{ds}\right)_- = \frac{1}{u-a}. \tag{3.5}$$

The characteristic equations are

$$\frac{d}{dt}\left(\ln \rho + \frac{V_s}{a}\right) = A + \frac{B}{a} \text{ along } \frac{dt}{ds} = \frac{1}{u+a} \tag{3.6a}$$

and

$$\frac{d}{dt}\left(\ln \rho - \frac{V_s}{a}\right) = A - \frac{B}{a} \text{ along } \frac{dt}{ds} = \frac{1}{u-a}. \tag{3.6b}$$

where

$$A = -V_s \frac{\partial \theta}{\partial n} + V_n / R - \frac{\partial V_n}{\partial n} \tag{3.6c}$$

and

$$B = -g \cos \theta + V_n \frac{D\theta}{Dt} + \frac{V_n V_s}{R} \tag{3.6d}$$

We assumed an initial hydrostatic state given by

$$V_n = 0, \tag{3.7a}$$

$$V_s = 0 \tag{3.7b}$$

and

$$\rho(s) = \rho(0) \left\{1 - g \frac{[z(s) - z(0)]\ (\Gamma - 1)}{a^2(0)}\right\}^{1/(\Gamma-1)} \tag{3.7c}$$

4. Method of Solution

A numerical method was used to integrate equations (3.6a) and (3.6b). In this method all the flow properties were determined at prespecified grid points using an inverse marching method (Zuorow and Hoffman, 1976). For illustration, the procedure for determining the velocity and pressure at an interior point d is described, given the properties at three other space points a, b and c at an earlier instant of time (see Figure 1). If we

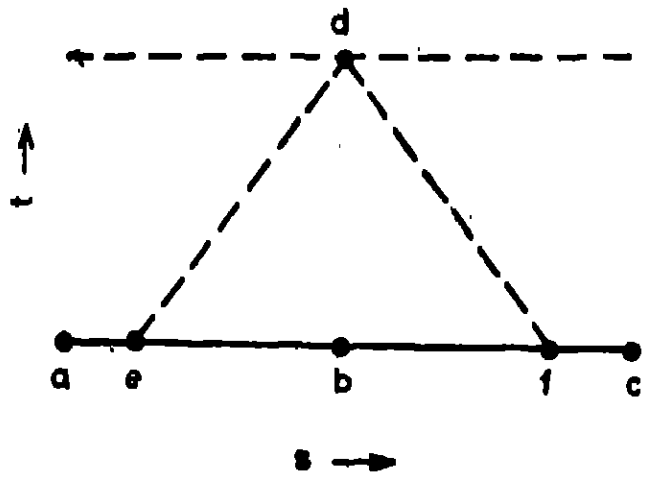

Fig. 1. Inverse marching for interior point d. a b c is the previous time–line: de and df are the right and left running characteristics, respectively.

draw characteristics from d towards the previous time line, they will meet it at two points, say e and f respectively. Flow properties along the right running characteristic will be subscripted, in what follows, with a + sign and the −sign given for variables on the left running characteristic. If we cast the equations (3.5), (3.6a) and (3.6b) in finite difference form, we get

$$(s_d - s_e) = \Delta t\,(u_+ + a_+)\,; \tag{4.1a}$$

$$(s_d - s_f) = \Delta t\,(u_- - a_-)\,; \tag{4.1b}$$

$$\ln\left(\frac{\rho_d}{\rho_e}\right) + \frac{(u_d - u_e)}{a_+} = \Delta t\, y_+\,; \tag{4.1c}$$

$$\ln\left(\frac{\rho_d}{\rho_f}\right) - \frac{(u_d - u_f)}{a_-} = \Delta t\, y_-\,; \tag{4.1d}$$

where $Y_+ = A_\pm \pm B_\pm/a_\pm$

and Δt is the time step which was chosen such that it did not violate the Friedrichs-Courent-Lewy criterion.

Since the flow properties and location of points e and f are not known, these equations must be solved iteratively. An Euler predictor-corrector method was used for the iteration.

For the predictor algorithm we chose initially:

$$u_+^{(0)} = u_a,\quad p_+^{(0)} = p_a,\quad u_-^{(0)} = u_a,\quad p_-^{(0)} = p_a$$

and likewise for the geometric parameters. These were used in equations (4.1a) and (4.1b) to obtain a first guess for the location of points e and f. The flow properties at these points were determined by interpolating between the values at points a, b and c. For subsequent iterations in the predictor we assumed:

$$u_+^{(n)} = u_e^{(n-1)},\quad p_+^{(n)} = p_e^{(n-1)},\quad u_-^{(n)} = u_f^{(n-1)},\quad p_-^{(n)} = p_f^{(n-1)}$$

where the superscripts denote the order of the iteration. When the calculated value of s_e and s_f converged to a specified tolerance, the latest values of $u_\pm$ and $p_\pm$ were used to calculate the properties at point d from equations (4.1c) and (4.1d). In the present study, a relative convergence to within 10^{-4} was found to be generally attained within five iterations.

Next, the corrector was applied to the above predicted values of u_d and p_d. For the corrector we assumed

$$u_+ = \frac{(u_e + u_d)}{2}\,,\quad p_+ = \frac{(p_e + p_d)}{2}\,,$$

$$u_- = \frac{(u_f + u_d)}{2}\,,\quad p_- = \frac{(p_f + p_d)}{2}\,.$$

Here too, an iteration is required to locate points e and f as well as to determine the flow properties. However, during this iteration, the values of u_d and p_d (which were determined by the predictor) are not changed. After obtaining convergence, u_d and p_d are redetermined. To improve the accuracy we substituted these corrected values of u_d and p_d back into equations (4.1) and followed the same steps mentioned above to obtain improved values. The maximum number of predictor iterations was limited to five and the corrector was applied at most three times.

4.1 Boundary Conditions

The method just described is only applicable to an interior point. It is well known for time-dependent initial value problems solved by the method of characteristics, that the number of boundary conditions necessary to solve the problem uniquely is $2-n$, where n is the number of characteristics crossing the boundary from an

interior point. In the present case, the left characteristic does not cross the right boundary and the right characteristic does not cross the left boundary. Hence we require one boundary condition each at the two boundaries. We used two different conditions for the left (lower) boundary, namely

$$u = a\,(1 - e^{-t/\tau}) \tag{4.1.1}$$

or

$$p = \text{constant}. \tag{4.1.2}$$

For the right (top) boundary we prescribed the value of u extrapolated from two preceeding space points. This boundary condition assured a smooth termination of the spatial velocity and pressure runs. The equation relating p_d and u_d along the "missing" characteristic is replaced by the boundary condition which prescribes any one of u_d and p_d. The remaining variable is then determined from the rest of equations (4.1).

4.2 Correction for Distortion of Grid Due to Stretching of Field Lines

The prescribed lateral velocity stretched the field lines at every instant of time. This brought on the complication of grid distortion. To eliminate this, we calculated the geometric parameters of the line at certain points which followed the natural motion of the line. The equations for the displacement of these points are given by

$$\frac{dy}{dt} = V_n \cos\theta\,; \tag{4.2.1a}$$

$$\frac{dz}{dt} = -V_n \sin\theta\,; \tag{4.2.1b}$$

$$\frac{d\theta}{dt} = \frac{\partial V_n}{\partial s}\,; \tag{4.2.1c}$$

$$\Delta s = \int_{z(t)}^{z(t+\Delta t)} \frac{dz}{\cos\theta}\,; \tag{4.2.1d}$$

$$\frac{1}{R} = \cos\theta\,\frac{\partial\theta}{\partial z}\,; \tag{4.2.1e}$$

where Δs is the total displacement in a time Δt. Equations (4.2.1a) through (4.2.1c) were integrated using an Euler predictor-corrector method with a time step $\delta t = \Delta t/3$ to achieve improved accuracy. The integration and differentiation in equations (4.2.1d) and (4.2.1e) were performed using Lagrange 3-point interpolation formulae (Abramowitz and Stegun, 1965). Having obtained the coordinates and geometric parameters at the displaced points, we determined them at the original spatial grid points by Lagrange 3-point interpolation. Hence the problems involved in a moving grid (like non-uniform spatial step size) could be eliminated.

5. Choice of the Lateral Flow

In order to keep the study sufficiently general, the following two forms for the lateral velocity V_n were considered:

$$\text{I)}\quad V_n = V_0 \exp z/H\,; \tag{5.1}$$

where V_0 and H are constants.

$$\text{II)}\quad V_n = V_b(t)\,\sin ky / \sin ky_b(t)\,; \tag{5.2}$$

where $V_b(t) = V_0 \sin ky_b(t) \cos ky_b(t)/\sin ky_b(0)$ is the velocity of the base point, $y_b(t) = 2\,y_b \tan^{-1}\left(\exp\left(-V_b\,(t - t_a)/y_b\right)\right)$ is its y - coordinate, V_0 is a constant and y_b and t_a are given by

$$y_b = 2y_b(0)/\pi,\quad t_a = 0;\quad t = \tau$$

and

$$y_b = 2y_b(\tau)/\pi,\ t_\tau = \tau,\ t > \tau.$$

The form (5.1) was chosen for simplicity. The symbol H denotes the scale height of the velocity variation, which can be either positive or negative. The form (5.2) ensured that the geometry of the field lines was conserved such that the relation $\theta = ky$ was satisfied at all times. This enabled us to calculate the equation of the streamline analytically at each instant of time. The velocity of the base point was chosen to have an initial rapid motion followed by a decrease to almost zero velocity. Such a motion simulates a rapid onset of some instability and its subsequent quenching by the enhancement of the magnetic field. Figure 2 depicts the boundary of a field line moving with such a velocity.

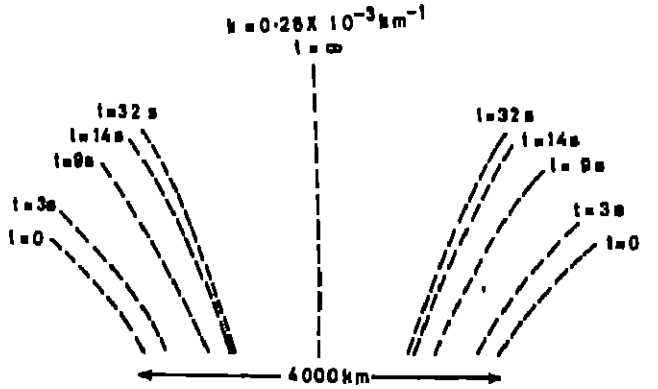

Fig. 2 The streamlines (or magnetic field lines) at different instants of time when the flow was according to (5.2). An initial value $V_{nb} = 60$ km s^{-1} was assumed for the base velocity.

6. Description of Results

For purposes of computation, we chose $R = 8.2 \times 10^7$ and temperatures of the order of 10000 K, which are typical of the solar chromosphere and a representative field length of 2000 km. We see that the choice of base temperature does not critically affect the basic nature of the flow. Hence, the description of results that follows is applicable for different temperatures as well.

The equations (3.6a, b) were first solved using the form for the normal velocity given by equation (5.1). The results exhibited several interesting features. The most obvious one is that the parallel flow is always initiated in the direction of increasing $|V_n|$. Figure 3 shows this result explicitly for $\Gamma = 1$ (isothermal flow). Here the value of V_n at the base is 10 km s^{-1} for the case where it increases in the positive s-direction whereas the base velocity is set equal to 60 km s^{-1} in the case where $|V_n|$ decreases with s. The scale height of variation in both cases is 1000 km.

There is no drastic change in the flow properties when different values of Γ, the polytropic index are assumed. In Figure 4, the results are depicted for five values of Γ (including the isothermal case) for a base temperature ~5000 K and a base velocity V_n ~500 m s^{-1}. The scale height of velocity variation is 500 km with $|V_n|$ decreasing with height. In all cases there are downdrafts for all times except for the single case where $\Gamma < 1$ (simulating temperature increasing with height). Even in this exceptional case, the behaviour after a sufficiently long time tends to be similar to the other four cases. Hence, using $\Gamma = 1$ for the subsequent computations does not lead to any loss of generality.

Consider now the second form for V_n according to equation 5.2. In this case, the direction of parallel flow is once again along the direction of increasing $|V_n|$. The effect of boundary conditions and initial conditions can be easily discerned in figures 5 and 6 where the spatial velocity and pressure (or density) runs for three

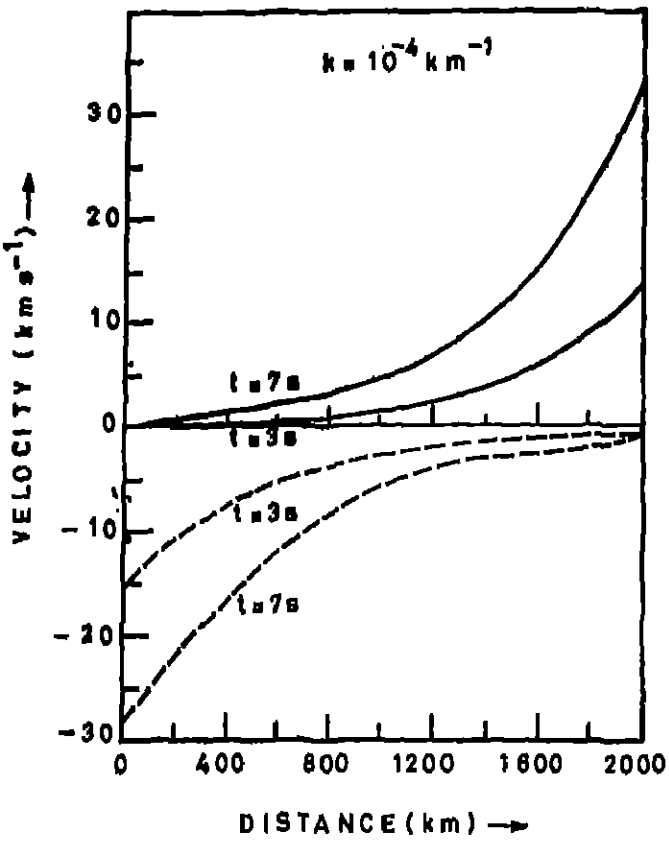

Fig. 3 The run of parallel velocity at different times is shown for H = −1000 km and V_{nb} = 80 km s^{-1} (at t=0) by solid lines, and H=1000 km, V_{nb} = 10 km s^{-1} (at t=0), represented by dashes.

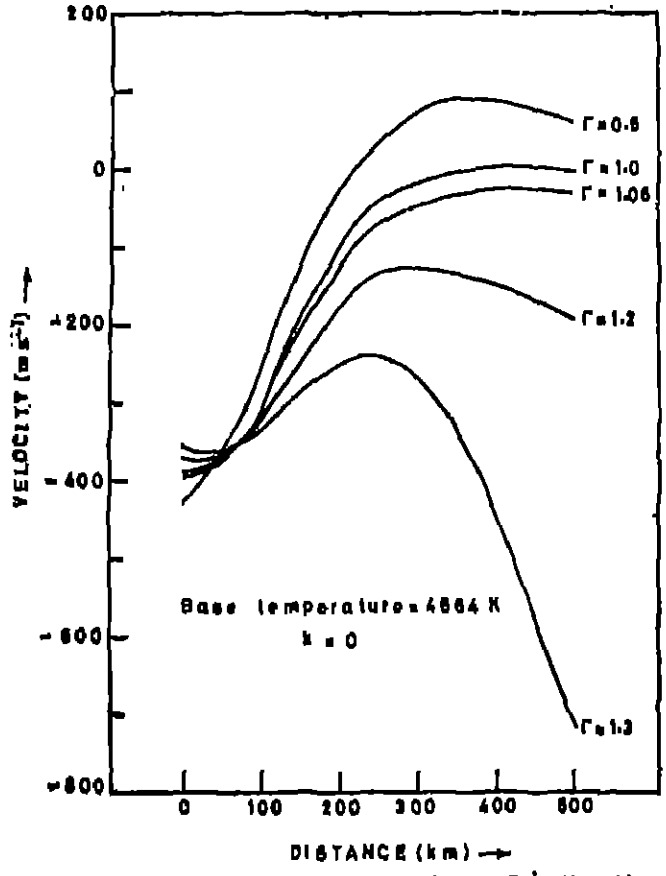

Fig. 4 Run of velocity for five values of Γ (Γ=0.8, 1.0, 1.05, 1.2 and 1.3) at t=32s. Here V_{nb} = 500 m s^{-1}, and H=−500 km

different instants of time are shown. A small kink can be seen propagating downstream with a velocity approximately equal to 25 km s^{-1}. At later times, a second kink is also seen. The first kink could be due to the initial condition of sudden onset of the lateral flow while the second peak could be due to the boundary condition (4.2.1) where we prescribe the parallel velocity V_z at the base. This is borne out by Figures 7 and 8 where a smoother boundary condition of constant base pressure is assumed. Here we see only one kink which propagates downstream with a speed of roughly 15 km s^{-1}. We identify this kink as the one due to the initial conditions. Table 1 gives the positions of the kinks at various instants of time. Figures 9 and 10 show the temporal behaviour of the velocity and pressure at two different space points with boundary conditions (4.2.1)

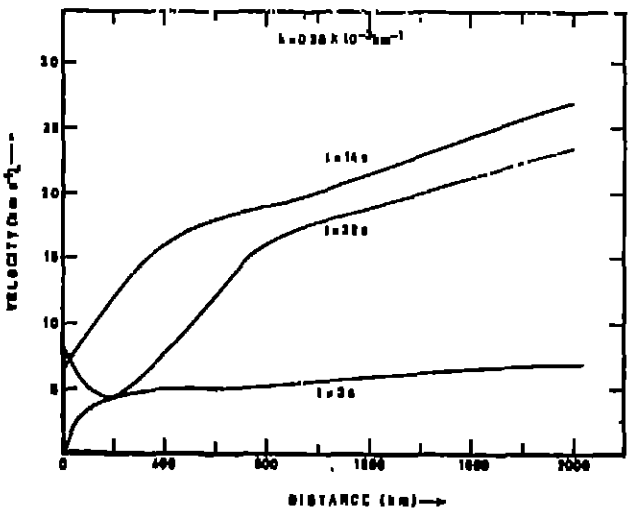

Fig. 6 The spatial variation of parallel velocity at different times is shown for an initial choice V_{nb} = 60 km s^{-1} with the boundary condition (4.1.1).

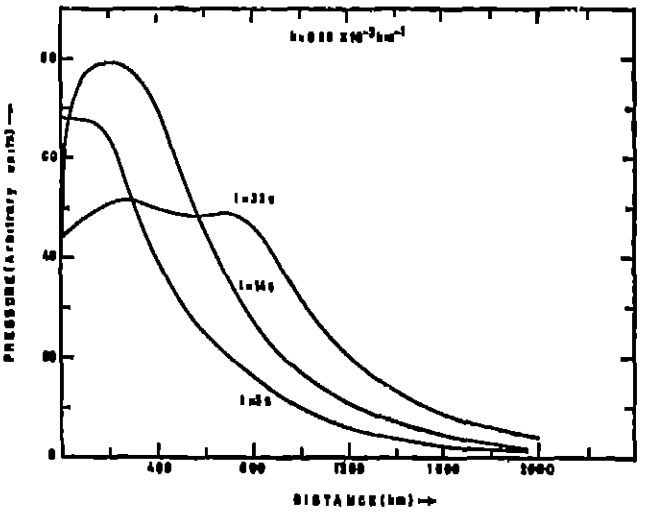

Fig. 8 The spatial variation of pressure (density) at different times for an initial choice V_{nb} = 60 km s^{-1} with boundary condition (4.1.1).

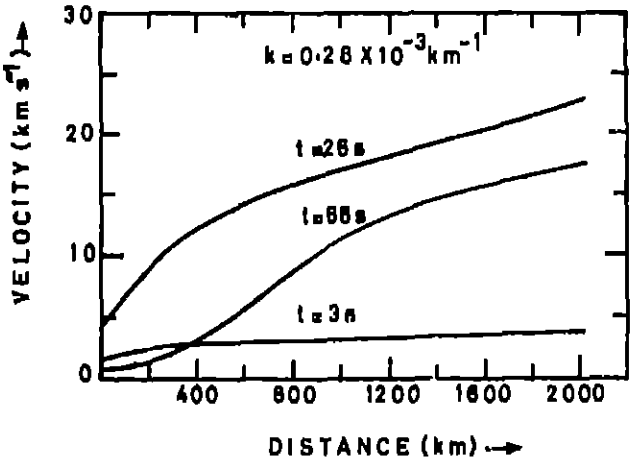

Fig. 7. Spatial variation of velocity at different times for an initial choice V_{nb} = 60 km s^{-1} with boundary condition (4.1.2).

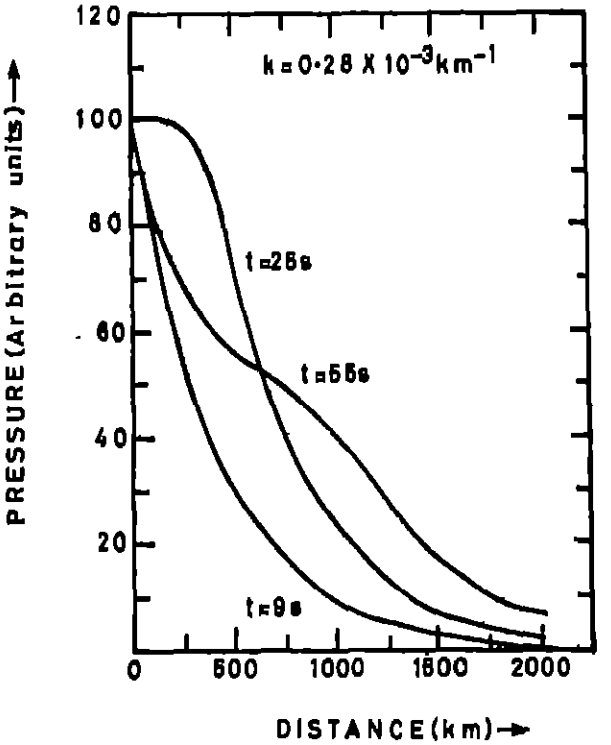

Fig. 8 Spatial variation of pressure (density) at different times for an initial choice V_{nb} = 60 km s^{-1}, with boundary condition (4.1.2).

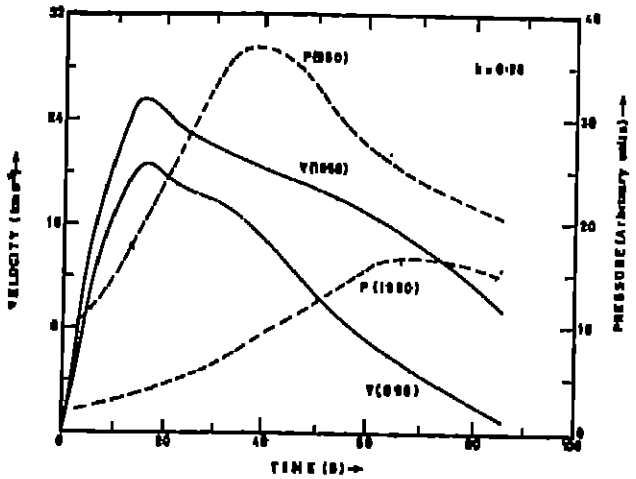

Fig. 9 Time variation of velocity (solid lines) and pressure/density (dashes) for V_{nb} = 80 km s^{-1}, with boundary condition (4.1.1).

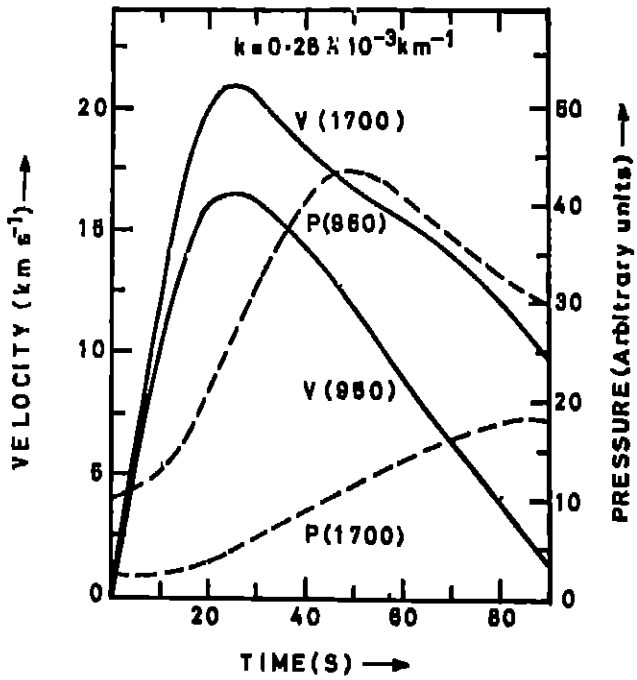

Fig. 10 Time variation of velocity (solid lines) and pressure density (dashes) for V_{nb} = 60 km s^{-1}, with boundary condition (4.1.2).

Table 1. Approximate positions of velocity and pressure kinks of Figs. 5, 6, 7 and 8 at different instants of time. Appearance of two values in a column indicates two kinks.

Figure No.	Time (s)	Position of Pressure kink (km)	Position of Velocity kink (km)	Velocity of propagation of kink (km s^{-1})	
				Velocity	Pressure
	3	0	100	—	—
5/6	14	300	400	27	27
	32	600,300	800,0	22	28
	3	0	200	—	—
7/8	25	300	600	18	14
	55	800	1000	13	17

and (4.2.2) respectively. In both cases there is a rise to peak velocity followed by a decline. The decline is due to the rapid diminution of the lateral flow around 20 seconds. The peak velocities are different since the initial values for V_n at the base are different (equal to 80 km s^{-1} respectively). We find that smaller starting values for V_n produces smaller parallel flows. The decline of the parallel flow is on a time scale comparable to the acoustic travel time over the length of the field line participating in the lateral motion. For a total length of 2000 km for the field line, the time scale of decline is approximately 70s. Figure 11 shows the temporal behaviour of the parallel flow when a field line of length 4000 km is considered. The behaviour is similar to that in the shorter field line, but the decline of the parallel flow indicates a relaxation time of approximately 300 seconds. The behaviour of the lateral flow V_n is also plotted alongside for the sake of illustration. The effect of curvature of field lines can be seen clearly in Figure 12. The larger the curvature, the larger is the peak velocity attained.

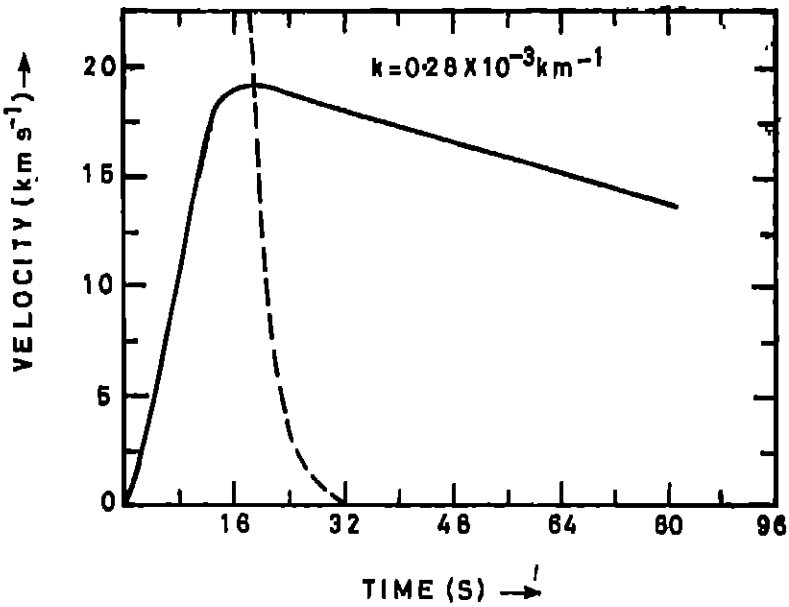

Fig. 11. Time variation of parallel velocity (solid line) and normal velocity (dashes) at s=2900 km for a total field length of 4000 km and V_{nb} = 60 km s^{-1}, boundary condition (4.1.2) was used.

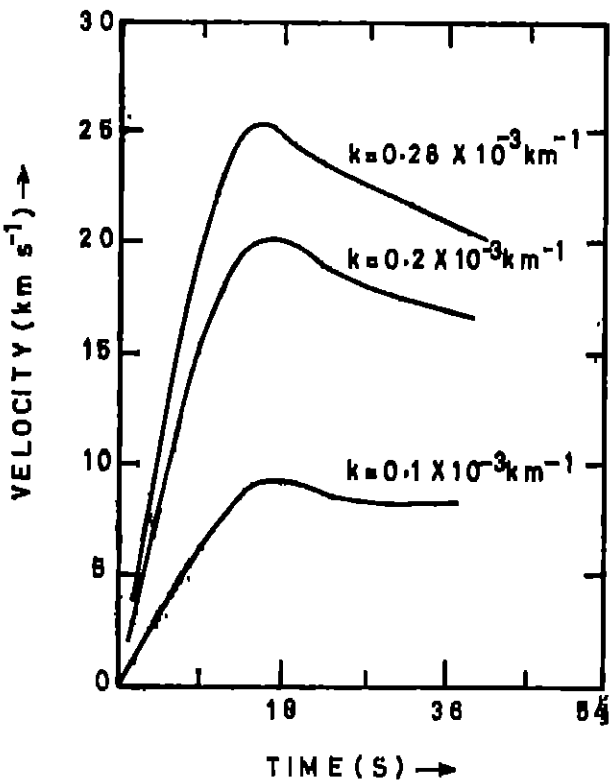

Fig. 12. The effect of curvature on the temporal distribution of velocity at s=1700 km is depicted. A value of 20000 K for the temperature and an initial normal velocity V_{nb} =80 km s^{-1} were used.

7. Conclusions and Discussion

The main results obtained from the present study are :

1) For the range of polytropic indices considered, the gas is accelerated in the direction of increasing lateral velocity.

2) The peak velocity attained by the parallel flow depends on the magnitude of the initial base velocity of the lateral flow.

3) The larger the curvature of the field line, the greater is the peak velocity attained by the parallel flow.

4) The relaxation time for the decline of the parallel flow (in the absence of the lateral flow) depends on the length of field line considered.

5) The basic nature of the flow is not greatly influenced by the choice of base temperature or polytropic index.

Results (1) through (3) can be simply understood as due to the dominance of the term $V_n \frac{D\delta}{Dt}$ in equation (3.3). The non-uniform lateral motion of a line element imposes on the associated fluid element: (1) a translational motion of its centre of gravity along a curved path and (2) a rotation around the centre of gravity. The term $V_n \frac{D\delta}{Dt}$ can then be interpreted as a centrifugal acceleration due to the translational motion along the curved path (centrifugal forces due to rotation of the line element cancel out when integrated over the field line.) The direction of this centrifugal acceleration is in the direction of increasing $|V_n|$. Moreover, the magnitude of the acceleration will depend both on the magnitude of V_n and the amount of curvature of the field line. The dependence of the relaxation time on the length of the field line can be understood in terms of the finite time taken for pressure disturbances to traverse the length of the line. Finally the weak dependence of the flow on the temperature indicates that the flow does not cause any major alteration in the balance between gravity and the pressure gradient.

8. Applications

On the Sun, there are several kinds of flow situations. According to Deubner (1975), very large downdrafts ($\sim 2\,\mathrm{km\,s^{-1}}$) can be inferred to be present in the dark intergranular lanes. There are downdrafts (~ 100 to $200\,\mathrm{m\,s^{-1}}$) at the borders of supergranulation cells and it is generally agreed that the main downdrafts occur in very localised magnetic regions at the cell boundary (Bohm, 1976; Giovanelli, 1980). There are also strong downflows ($\sim 3\,\mathrm{km\,s^{-1}}$) associated with the birth of sunspots and active regions (Zwaan, 1978) which have been modelled in terms of matter sliding down along rising magnetic flux tubes (Shibata, 1980). For examples of outward flows (or updrafts) we have spicules in the chromosphere and high speed solar wind streams presumably originating in coronal holes. All these flows have the common property of being highly localised and in all probability are channelled by magnetic fields. It is not unrealistic to think of situations where a change in the field geometry can take place, for example by means of hydromagnetic or thermal instabilities, or "buffeting" of the field lines by external flows. The present study shows the extent of the resulting parallel flow given the magnitude of the lateral flows. Conversely, it indicates the magnitude of the lateral flows necessary if the observed flows are in fact caused by changes in the magnetic field geometry.

9. Summary

The time variation of the shape of a magnetic field line produces a centrifugal acceleration along the line. This acceleration induces gas flow along the magnetic field. There are several flows observed on the Sun, which could be a manifestation of such a time variation in the magnetic field geometry and this study indicates the degree of variation required to cause the flows.

A, 1965, *Handbook of Mathematical Functions*, Dover, New York, p. 875.
B, *Problems of Stellar Convection*, Eds E.A. Spiegel and J.P. Zahn, Springer-Verlag, Berlin, p. 103
hys. 44, 371.
Giovanelli, R.G. 1980, *Solar Phys.* 67, 211.
Kopp, R.A. Pneuman, G.W. 1976, *Solar Phys.* 50, 85.
Shibata, K. 1980, *Solar Phys.* 68, 61.
Zuorow, M.J., Hoffman, J. D. 1976, *Gas Dynamics*, John Wiley, New York, p. 36.
Zwaan, C. 1978, *Solar Phys.* 60, 213.